

Functional Properties of Endogenous Receptor- and Store-operated Calcium Influx Channels in HEK293 Cells*

Received for publication, January 6, 2005, and in revised form, February 28, 2005
Published, JBC Papers in Press, March 1, 2005, DOI 10.1074/jbc.M500192200

Vladislav Bugaj‡, Vadim Alexeenko‡, Alexander Zubov‡, Lyuba Glushankova‡, Anton Nikolaev‡, Zhengnan Wang§, Elena Kaznacheyeva‡, Ilya Bezprozvanny§¶, and Galina N. Mozhayeva‡¶

From the ‡Institute of Cytology RAS, 4 Tikhoretsky Avenue, St. Petersburg 194064, Russia and the §Department of Physiology, University of Texas Southwestern Medical Center, Dallas 75235

Activation of phospholipase C (PLC)-mediated signaling pathways in non-excitabile cells causes the release of calcium (Ca^{2+}) from inositol 1,4,5-trisphosphate (InsP_3)-sensitive intracellular Ca^{2+} stores and activation of Ca^{2+} influx via plasma membrane Ca^{2+} channels. The properties and molecular identity of plasma membrane Ca^{2+} influx channels in non-excitabile cells is a focus of intense investigation. In the previous studies we used patch clamp electrophysiology to describe the properties of Ca^{2+} influx channels in human carcinoma A431 cell lines. Now we extend our studies to human embryonic kidney HEK293 cells. By using a combination of Ca^{2+} imaging and whole cell and single channel patch clamp recordings we discovered that: 1) HEK293 cells contain four types of plasma membrane Ca^{2+} influx channels: I_{CRAC} , I_{min} , I_{max} , and I_{NS} ; 2) I_{CRAC} channels are highly Ca^{2+} -selective ($P_{\text{Ca/Cs}} > 1000$) and I_{CRAC} single channel conductance is too small for single channel analysis; 3) I_{min} channels in HEK293 cells display functional properties identical to I_{min} channels in A431 cells, with single channel conductance of 1.2 pS for divalent cations, 10 pS for monovalent cations, and divalent cation selectivity $P_{\text{Ba/K}} = 20$; 4) I_{min} channels in HEK293 cells are activated by InsP_3 and inhibited by phosphatidylinositol 4,5-bisphosphate, but store-independent; 5) when compared with I_{min} , I_{max} channels have higher conductance for divalent (17 pS) and monovalent (33 pS) cations, but less selective for divalent cations ($P_{\text{Ba/K}} = 4$), 6) I_{max} channels in HEK293 cells can be activated by InsP_3 or by Ca^{2+} store depletion; 7) I_{NS} channels are non-selective ($P_{\text{Ba/K}} = 0.4$) and display a single channel conductance of 5 pS; and 8) I_{NS} channels are not gated by InsP_3 but activated by depletion of intracellular Ca^{2+} stores. Our findings provide novel information about endogenous Ca^{2+} channels supporting receptor-operated and store-operated Ca^{2+} influx pathways in HEK293 cells.

Activation of phospholipase C (PLC)¹-mediated signaling pathways in non-excitabile cells causes the release of calcium (Ca^{2+}) from inositol 1,4,5-trisphosphate (InsP_3)-sensitive intracellular Ca^{2+} stores and activation of Ca^{2+} influx via plasma membrane Ca^{2+} channels. Receptor-operated (ROC) and store-operated (SOC) Ca^{2+} influx pathways have been described in non-excitabile cells (1–3). ROC Ca^{2+} influx pathways are activated directly as a result of PLC-coupled receptor activation. Activation of SOC Ca^{2+} influx pathways requires depletion of intracellular Ca^{2+} stores. Functional properties and molecular identity of channels supporting ROC and SOC Ca^{2+} influx pathways is a focus of intense investigation. Based on their selectivity for divalent cations, SOC currents can be separated into highly Ca^{2+} -selective channels ($P_{\text{D/M}} > 1000$) named “ Ca^{2+} release-activated channels” (I_{CRAC}) (4–6) and moderately Ca^{2+} -selective ($P_{\text{D/M}} \sim 10$) channels I_{SOC} (1–3,7). The molecular identity of I_{CRAC} remains unclear (1–3,8). Mammalian *trp* channels of the TRPC family are the most likely candidates for the role of I_{SOC} channels (3, 7, 9–12). Properties of ROC channels are much less understood due to the difficulty in separating direct effects of PLC activation from effects resulting from depletion of intracellular InsP_3 -sensitive Ca^{2+} stores.

Most of the functional studies of ROC and SOC Ca^{2+} influx pathways have been performed using Ca^{2+} imaging or whole cell current recordings. We reasoned that single channel patch clamp recordings provide unique and precise information about functional properties of individual types of channels supporting Ca^{2+} influx in non-excitabile cells. In our previous experiments we used single channel patch clamp recordings to perform detailed characterization of channels supporting Ca^{2+} influx in A431 cells (13–19). Now we extended our studies to HEK293 cell line, which is used extensively as heterologous expression host in functional studies of TRPC family members, such as TRPC1 (20), TRPC3 (21–23), TRPC4 (24), TRPC5 (20, 23, 25), TRPC6 (26, 27), and TRPC7 (27). HEK293 cells express endogenous TRPC1, TRPC3, TRPC4, and TRPC6 proteins (28–30), and the functional properties of endogenous Ca^{2+} influx channels in HEK293 cells described here will be useful for interpretation of results obtained in heterologous expression studies of TRPC channels in HEK293 cells. Obtained results also provide interesting insights into similarities and differences between Ca^{2+} influx pathways in A431 and HEK293 cells.

* This work was supported by the program of “Molecular and Cellular Biology” Russian Academy of Science (to G. N. M.), the Russian Basic Research Foundation 04-04-49057 (to E. K.), 04-04-49053 (to G. N. M.), SS-2178.2003.4 (to G. N. M.), the National Institutes of Health Grant NS38082 (to I. B.), and the US Civilian Research and Development Foundation RB1-2018 (to G. N. M. and I. B.). The costs of publication of this article were defrayed in part by the payment of page charges. This article must therefore be hereby marked “advertisement” in accordance with 18 U.S.C. Section 1734 solely to indicate this fact.

¶ To whom correspondence may be addressed: Dept. of Physiology, K4.112, University of Texas Southwestern Medical Center, 5323 Harry Hines Blvd., Dallas, TX 75235-9040. Tel.: 214-648-6737; Fax: 214-648-8879; E-mail: Ilya.Bezprozvanny@UTSouthwestern.edu.

¶ To whom correspondence may be addressed. Tel.: 812-247-1497; Fax: 812-247-0341; E-mail: gnmzh@mail.cytspb.rssi.ru.

¹ The abbreviations used are: PLC, phospholipase C; InsP_3 , inositol 1,4,5-trisphosphate; PIP_2 , phosphatidylinositol 4,5-bisphosphate; ROC, receptor-operated Ca^{2+} influx pathway; SOC, store-operated Ca^{2+} influx pathway; I_{CRAC} , Ca^{2+} release-activated channel; R, receptor; *c/a*, cell-attached; *i/o*, inside-out; Ad- InsP_3 R-N, adenovirus encoding the InsP_3 -binding amino-terminal region of rat InsP_3 R1; Ab, antibody; BAPTA-AM, 1,2-bis(2-aminophenoxy)ethane-*N,N,N',N'*-tetraacetic; TPEN, *N,N,N',N'*-tetrakis(2-pyridylmethyl)ethylene diamine; TRPC, canonical transient receptor potential.

EXPERIMENTAL PROCEDURES

Cell Culture—HEK293 cells (Cell Culture Collection, Institute of Cytology, St. Petersburg, Russia) were cultured in Dulbecco's modified Eagle's medium supplemented with 10% fetal bovine serum, 100 units/ml penicillin, 100 μg/ml streptomycin, and 2 mM glutamine. Cells were grown in an incubator at 37 °C with humidified 5% CO₂ and 95% air. For patch clamp and Ca²⁺ imaging experiments cells were seeded onto coverslips and maintained in culture for 1–3 days before use.

Generation of Recombinant Adenoviruses—Ad-InsP₃R-N adenovirus was generated using the AdEasy system according to published procedures (31). Briefly, an amino-terminal fragment of rat InsP₃R1 (32) (M1-K604) was amplified by PCR (with addition of 5'-untranslated region Kozak sequence and carboxyl-terminal His₆ tag) and subcloned into KpnI/XhoI sites of pAdTrack-CMV shuttle vector. Resulting pAdTrack-CMV-InsP₃R-N plasmid was linearized by PmeI and co-transformed into *Escherichia coli* BJ5183 cells together with pAdEasy-1 adenoviral backbone plasmid. Recombinants were selected by kanamycin resistance and confirmed by PCR analysis. Recombinant adenoviral plasmid pAd-InsP₃R-N was isolated, linearized by PacI, and transfected into HEK293 cells for packaging. Transfected cells were monitored for GFP expression, collected 10 days after transfection, and lysed by three cycles of rapid freezing and thawing in methanol/dry ice bath. Collected viral lysate (P1) was clarified by centrifugation and high titer (P3) stock of Ad-InsP₃R-N adenovirus was obtained by repetitive rounds of HEK293 cell infection. Obtained high titer stock of Ad-InsP₃R-N adenovirus was aliquoted, frozen at -70 °C and transported on dry ice from Dallas, TX, to St. Petersburg, Russia for experiments.

Ca²⁺ Imaging—HEK293 cells grown on glass coverslips were loaded with 5 μM Fura-2AM in the presence of 0.025% Pluronic for 20–30 min. Loaded cells were illuminated by alternating 340 and 380 nm excitation light at 2-Hz frequency. Emission fluorescence intensity was measured at 510 nm with the use of an InCyt Basic I/P dual wavelength fluorescence imaging system (Intracellular Imaging Inc., Cincinnati, OH). The change of cytosolic Ca²⁺ concentration in cells was expressed as the ratio of emission fluorescence intensity at 340 and 380 nm excitation wavelengths (340/380 ratio). In experiments with recombinant adenovirus HEK293 cells were infected using high titer stock of Ad-InsP₃R-N 2–3 days prior to Ca²⁺ imaging experiments. The efficiency of infection was close to 100% based on GFP fluorescence.

Whole Cell Recordings—Whole cell recordings were performed using an Axopatch 200B patch clamp amplifier (Axon Instruments) with a conventional 10-GΩ feedback resistance in the head stage. Resistance of Sylgard-coated, fire-polished glass microelectrodes was 3–5 MΩ. Series resistance was not compensated. The pipette solution contained (in mM) 145 N-methyl-D-glutamine aspartate, 10 Cs-EGTA (or 12 Cs-BAPTA), 10 Cs-HEPES, pH 7.3, 1.5 MgCl₂, and either 4.5 CaCl₂ (pCa 7.0) or no CaCl₂ added (pCa > 9). Extracellular solution contained (in mM) 140 N-methyl-D-glutamine aspartate, 10 BaCl₂, 10 Cs-HEPES, pH 7.3. During recording the currents were sampled at 5 kHz and filtered digitally at 500 Hz. pClamp6 software suite (Axon Instruments) was used for data acquisition and analysis. In all whole cell experiments the holding potential was 0 mV. Periodically (once every 4–30 s) the membrane potential was stepped to -100 mV (for 30 ms), and a 170-ms voltage ramp to +70 mV was applied. Traces recorded before current activation were used as a template for leak subtraction. The recorded currents were normalized to the cell capacitance. The mean value of cell capacitance was 40 ± 5 pF (n = 41).

Single Channel Recordings—Single channel recordings were performed using an Axopatch 200B patch clamp amplifier and glass pipettes with 8- to 15-MΩ resistance. The pipette solution contained (in mM): 105 BaCl₂ or 140 NaCl as indicated and 10 Tris-HCl (pH 7.3). In cell-attached (c/a) experiments, the bath solution contained 140 mM KCl and 2 mM CaCl₂ to nullify the resting potential of the cell. In store depletion experiments 1 mM TPEN or 100 μM BAPTA-AM and 1 μM thapsigargin were added to the bath solution containing (in mM): 140 KCl, 5 NaCl, 10 K-Hepes, and 2 EGTA (pH 7.4). In inside-out (i/o) experiments the intracellular solution contained (in mM): 140 potassium glutamate, 5 NaCl, 1 MgCl₂, 10 K-HEPES, pH 7.4, 2 K-EGTA, and 1.13 CaCl₂ (pCa 7.0), with or without InsP₃ as indicated. The drugs were applied to the patches by bath perfusion. The time required for a complete change of solution around the patch was less than 1 s.

The single channel recordings were digitized at 5 kHz and filtered at 100 Hz for analysis and presentation. pClamp6 software suite (Axon Instruments) was used for data acquisition and analysis. Unitary current amplitude was determined from current records and all-point

amplitude histograms. The experiments were carried out at room temperature (22–24 °C).

P_{Ba/K} permeability ratio was calculated according to the GHK equation (33) (Equation 1),

$$P_{Ba/K} = [K_{in}]/4[Ba_{out}] \exp(E_{rev}F/RT) [\exp(E_{rev}F/RT) + 1] \quad (\text{Eq. 1})$$

where [K_{in}] is intracellular K⁺ concentration (140 mM), [Ba_{out}] is Ba²⁺ concentration in the pipette (105 mM), E_{rev} is the measured or extrapolated reversal potential, and RT/F = 25 mV for experiments performed at room temperature.

NPo was determined by using the following equation: NPo = {I}/i, where {I} and i are the mean channel current and unitary current amplitude, respectively. {I} was estimated from the time integral of the current above the baseline, and i was determined from current records and all-point amplitude histograms. Data were collected from current records after channel activity reached steady state. Because channel activity was transient and displayed significant fluctuations, we used NPo collected during 30 s of maximal activity (NPo₍₃₀₎) as a standard way to compare open channel probability among different experiments.

Chemicals—HEPES, EGTA, BAPTA-AM, N-methyl-D-glutamine, and TPEN were from Sigma-Aldrich; UTP and InsP₃ were from Calbiochem; and Fura-2AM and Pluronic were from Molecular Probes.

RESULTS

Store-operated and Receptor-operated Ca²⁺ Influx Pathways in HEK293 Cells—Application of 100 μM UTP to Fura-2-loaded HEK293 cells maintained in Ca²⁺-free media resulted in transient cytosolic Ca²⁺ elevation due to release of Ca²⁺ from intracellular InsP₃-sensitive Ca²⁺ stores (Fig. 1A). Subsequent re-addition of 2 mM extracellular Ca²⁺ resulted in second elevation of cytosolic Ca²⁺ due to Ca²⁺ entry via plasma membrane Ca²⁺ channels (Fig. 1A). Application of membrane-permeable low affinity Ca²⁺ chelator TPEN leads to rapid and reversible reduction of intraluminal Ca²⁺ concentration without disturbing cytosolic Ca²⁺ levels. We found that depletion of Ca²⁺ stores in HEK293 cells by 1 mM TPEN in Ca²⁺-free solution induces activation of Ca²⁺ influx following Ca²⁺ re-addition (Fig. 1B). Ca²⁺ influx induced by depletion of intraluminal Ca²⁺ (Fig. 1B) is a signature of store-operated Ca²⁺ (SOC) channels, which have been previously described in many non-excitable cells (1–3, 7). Thus, Ca²⁺ influx in response to UTP (Fig. 1A) can be mediated by plasma membrane receptor-operated Ca²⁺ (ROC) channels as a direct result of P2Y2 receptor activation or as result of SOC activation following depletion of InsP₃-sensitive intracellular Ca²⁺ stores. To determine if depletion of intracellular Ca²⁺ stores is required for UTP-induced Ca²⁺ influx, we infected HEK293 cells with an adenovirus encoding the InsP₃-binding amino-terminal region of rat InsP₃R1 (Ad-InsP₃R-N). Consistent with published observations (34), UTP-induced Ca²⁺ release was abolished in Ad-InsP₃R-N-infected cells (Fig. 1C), presumably due to ability of InsP₃R-N fragment to function as the "InsP₃ sponge" (34). Despite absence of Ca²⁺ release from InsP₃-sensitive stores, addition of extracellular Ca²⁺ resulted in Ca²⁺ influx in Ad-InsP₃R-N-infected cells exposed to UTP (Fig. 1C). Thus, we concluded that depletion of intracellular stores is not required for UTP-induced Ca²⁺ influx in HEK293 cells, which appear to be at least in part mediated by ROC channels.

Whole Cell Analysis of Ca²⁺ Influx Pathways in HEK293 Cells—In the next series of experiments we measured whole cell Ca²⁺ currents activated in HEK293 cells by extracellular UTP. We found that in some HEK293 cells (2 out of 8) application of UTP induced highly Ca²⁺-selective current with strong inward rectification (Fig. 2A). In other HEK293 cells (6 out of 8) the currents induced by UTP displayed linear current-voltage relationship with significant outward current at test potentials more positive than +30 mV (Fig. 2B). To characterize Ca²⁺ currents activated by depletion of intracellular Ca²⁺ stores, we repeated whole cell recordings with addition of 12

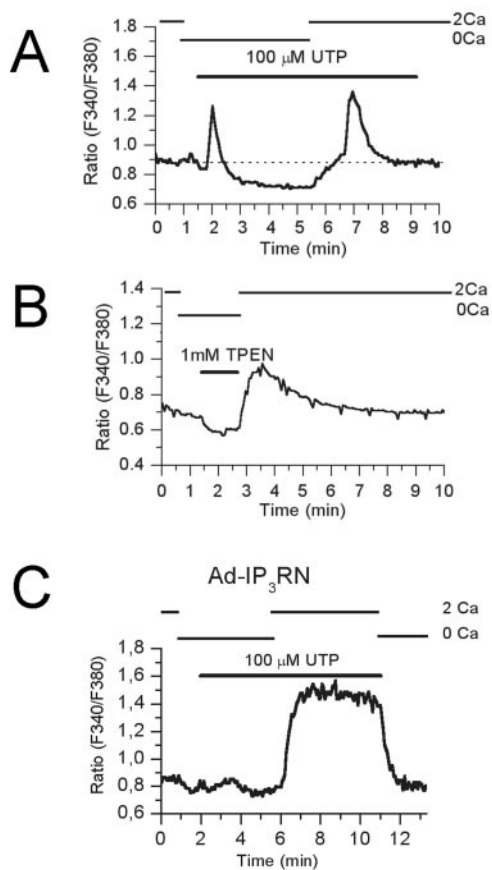


FIG. 1. Receptor- and store-operated Ca²⁺ entry in HEK293 cells. Cytosolic Ca²⁺ levels in HEK293 cells were monitored as 340/380 Fura-2 fluorescence ratio. The bars above indicate extracellular solution change between 0 and 2 mM Ca²⁺ and additions of 100 μM UTP or 1 mM TPEN. *A*, the Ca²⁺ release evoked by application of 100 μM UTP in Ca²⁺-free medium is followed by a Ca²⁺ elevation upon re-addition of Ca²⁺ to the extracellular medium. *B*, Ca²⁺ store depletion was induced by 1 mM TPEN added to the bath in the Ca²⁺-free medium. Subsequent re-addition of 2 mM extracellular Ca²⁺ resulted in Ca²⁺ entry. *C*, application of 100 μM UTP to HEK293 cells infected with Ad-InsP₃R-N adenovirus fails to induce Ca²⁺ release in Ca²⁺-free medium, but subsequent re-addition of 2 mM extracellular Ca²⁺ resulted in Ca²⁺ elevation due to Ca²⁺ entry. The data shown in panels A–C are representative of three to five experiments.

mm BAPTA into pipette. We found that in some cells (2 out of 12) depletion of Ca²⁺ stores induced highly Ca²⁺-selective current with strong inward rectification (Fig. 2C). In other cells (5 out of 12) less Ca²⁺ selective linear current was induced by store depletion (Fig. 2D). In our previous whole cell experiments with A431 cells we observed activation of highly Ca²⁺-selective (I_{CRAC}) and moderately Ca²⁺-selective (I_{SOCC}) currents by extracellular UTP and intracellular BAPTA (19). It appears that similar currents are also present in HEK293 cells (Fig. 2, A–D). In addition, some HEK293 cells (5 out of 12) express non-selective outwardly rectifying current activated by store depletion (Fig. 2E). This type of current was also rarely observed in whole cell experiments with A431 cells (data not shown).

I_{min} Channels Act as ROC Channels in HEK293 Cells—In the previous studies we utilized single channel patch clamp recordings to characterize Ca²⁺ influx channels in A431 cells (13–19). What are the channels supporting Ca²⁺ influx in HEK293 cells? To answer this question, we performed patch clamp recordings with HEK293 cells using 105 mM Ba²⁺ in the pipette as a current carrier. We found that application of 100 μM UTP to external surface of plasma membrane in cell-attached (*c/a*) patch evoked the activity of small conductance

channels in 56 out of 118 attempts (Fig. 3A). Channels with similar properties were activated by application of 2.5 μM InsP₃ to cytosolic surface of inside-out (*i/o*) patches (Fig. 3B) in 18 out of 80 experiments. The unitary current-voltage relationship of UTP-activated (in *c/a* experiments) and InsP₃-activated (in *i/o* experiments) channels is shown on Fig. 3C. The linear fit to the current-voltage relationship resulted in a slope conductance of 1.2 pS for both UTP-activated (Fig. 3C, filled symbols) and InsP₃-activated (Fig. 3C, open symbols) channels. The extrapolated reversal potential of these channels was equal to +50 mV (Fig. 3C), which corresponded to $P_{Ba/K} = 20$ (Equation 1) for ionic conditions used in our patch clamp experiments. Single exponential fit to the open dwell time distribution of UTP-activated channels yielded a mean open time of 9 ms (Fig. 3D). In our previous studies with A431 cells (13–15, 18, 19) we described UTP- and InsP₃-activated channels with similar conductance and gating properties, which we called “I_{min}.” Based on similarity in single channel properties (Table I) we concluded that HEK293 cells also express I_{min} channels that can be activated by UTP (in *c/a*) and InsP₃ (in *i/o*) (Table II).

I_{min} channels in A431 cells can also be activated by depletion of intracellular Ca²⁺ stores (18, 19). Does depletion of intracellular Ca²⁺ stores activate I_{min} channels in HEK293 cells? To answer this question we performed a series of *c/a* patch clamp recording experiments with HEK293 cells. In these experiments passive depletion of intracellular Ca²⁺ stores was induced by application of 1 mM TPEN in the bath ($n = 84$), loading cells with 100 μM BAPTA-AM in the presence of 1 μM thapsigargin in the bath ($n = 20$), or addition of 1 μM thapsigargin to the pipette solution ($n = 30$). Although these manipulations induced I_{min} activity in A431 cells (18, 19), none of these experiments yielded I_{min} activity in the *c/a* patches from HEK293 cells (Table II). Thus, we concluded that I_{min} channels in HEK293 cells are store-independent (Table I).

PIP₂ Inhibits I_{min} Channels in HEK293 Cells—Experiments described in the previous section led us to conclude that I_{min} channels in HEK293 cells function as InsP₃-gated ROC channels. What is a mechanism that couples PLC-coupled P2Y2 receptors with activation of I_{min} channels in intact cells? In the previous studies we proposed that I_{min} channels in A431 cells are functionally coupled to PLC-PIP₂-InsP₃R signaling complex (17, 18). Are I_{min} channels in HEK293 cells also coupled to PIP₂? To answer this question, we performed a series of inside-out (*i/o*) patch clamp experiments with anti-PIP₂ monoclonal antibodies (PIP₂Ab). We found that addition of PIP₂Ab facilitated the activity of InsP₃-gated I_{min} channels (Fig. 4A). By reversing the order of InsP₃ and PIP₂Ab additions to the patch, we established that PIP₂Ab alone was not sufficient for I_{min} activation but subsequent application of InsP₃ was effective in 48 of 60 experiments (Fig. 4B). Thus, InsP₃ was able to activate I_{min} channels in *i/o* patches pretreated with PIP₂Ab in 80% of experiments (48 out of 60), much higher than the 22% (18 out of 80) success rate in untreated patches (Table II). Thus, we reasoned that a large fraction of I_{min} channels in unstimulated HEK293 cells are under tonic inhibition by PIP₂. To test this hypothesis further, we repeated *i/o* experiments with addition of 100 μM UTP into the pipette solution. We reasoned that addition of UTP to the pipette will activate P2Y2 receptors in the patch leading to local hydrolysis of PIP₂ by PLC and relieve of I_{min} inhibition. Consistent with our expectations, addition of InsP₃ activated I_{min} channels in 7 out of 18 experiments (40%) when UTP was present in the pipette. Thus, addition of UTP in the pipette increased the success rate of I_{min} channels activation by InsP₃ from 22% to 40%. These results are in agreement with our previous studies of I_{min} activation mechanisms in A431 cells (17, 18), indicating that I_{min} channels in both A431

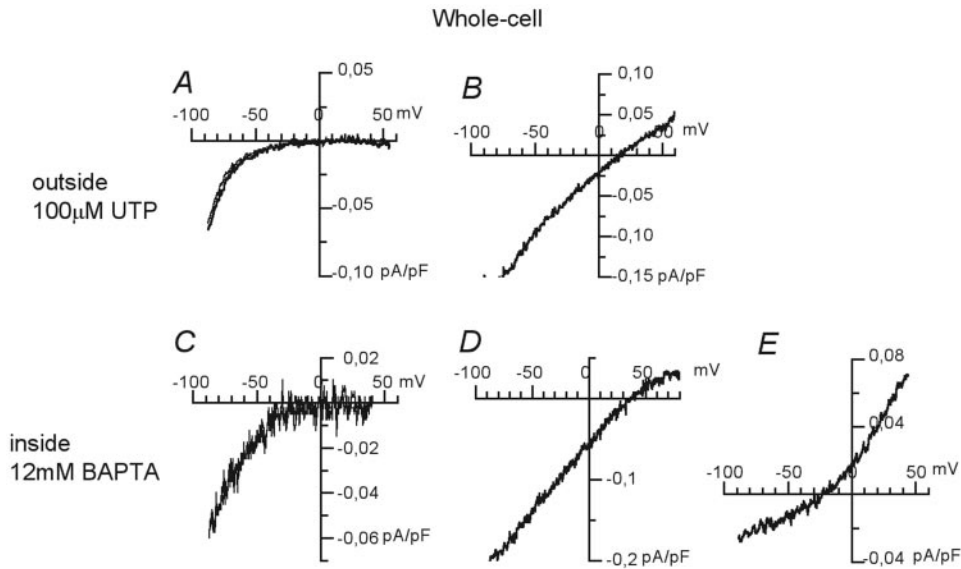


FIG. 2. Whole cell recordings of Ca²⁺ influx currents in HEK293 cells. *A* and *B*, current-voltage relationships of two types of currents after application of 100 μM UTP to HEK293 cells. *C–E*, current-voltage relationships of three types of currents recorded in HEK293 cells after passive Ca²⁺ store depletion by 12 mM BAPTA in the pipette solution. Data in each panel are representative for three to five experiments.

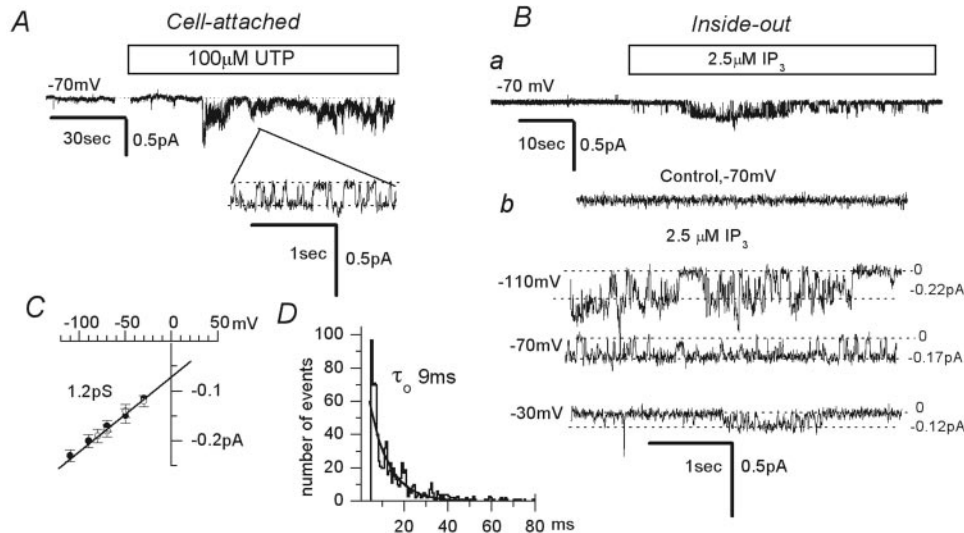


FIG. 3. I_{\min} channels in HEK293 cells. *A*, bath application of 100 μM UTP to cell-attached (*c/a*) patches held at -70 mV membrane potential activated I_{\min} channels in the patch. The fragments of current records are shown on the *bottom* on the expanded time scale. *B*, application of 2.5 μM InsP_3 to the cytosolic surface of inside-out (*i/o*) patch held at -70 mV membrane potential-activated I_{\min} channels in the patch (*a*). Expanded current traces of the records obtained prior to application of InsP_3 and after application of InsP_3 at membrane potentials as indicated are shown below (*b*). *C*, the mean current-voltage relationship of UTP (filled circles)- and InsP_3 (open circles)-activated I_{\min} channels. At each voltage the data are shown as mean \pm S.E. ($n = 6-8$). The liner fit to the data points (line) yields single channel conductance $\gamma = 1.2$ pS and extrapolated reversal potential $E_{\text{rev}} = +50$ mV. *D*, an open-time histogram of I_{\min} channel. One channel was active in the patch. Events with time duration of less than 3 ms were discarded to exclude artifactual openings from the analysis. The total number of events was 1170. The line represents a single exponential fit to the data with a time constant of $\tau_o = 9$ ms. Channel activity was recorded at membrane potential of -70 mV. Data were filtered at 500 Hz.

and HEK293 cells are inhibited by PIP_2 (Table I).

I_{\max} Channels Act as Both ROC and SOC Channels in HEK293 Cells—If I_{\min} channels in HEK293 cells are store-independent, then what channels support store depletion activated Ca²⁺ influx (Fig. 1*B*) in HEK293 cells? One possibility is that store-dependent Ca²⁺ influx in HEK293 cells is supported by highly Ca²⁺-selective I_{CRAC} channels (Fig. 2*C*). However, whole cell recordings revealed that in some cells depletion of intracellular Ca²⁺ stores causes activation of moderately Ca²⁺-selective I_{SOC} currents (Fig. 2*D*). Which channels mediate I_{SOC} currents in HEK293 cells? Examination of current records obtained in *c/a* experiments with HEK293 cells revealed that in 47 out of 118 experiments UTP activated channels with higher amplitude and different gating kinetics than I_{\min} (Fig. 5*A*). To

distinguish these channels from I_{\min} we called them “ I_{\max} .” Frequently ($n = 39$) I_{\min} and I_{\max} channels were observed in the same patch. For single channel analysis we selected *c/a* patches where only I_{\max} channels were observed in response to UTP ($n = 8$). Analysis of these experiments revealed that the unitary current-voltage relationship of I_{\max} channels was non-linear (Fig. 5*B*) with the slope conductance of 17 pS between -100 and -80 mV and 10 pS between -40 and -10 mV. The extrapolated reversal potential of I_{\max} channels was equal to $+30$ mV (Fig. 5*B*), which corresponded to $P_{\text{Ba/K}} = 4$ (Equation 1) for ionic conditions used in our patch clamp experiments. The open lifetime distribution of I_{\max} channels could be fitted by sum of two exponential functions with time constants $\tau_1 = 2.1$ ms and $\tau_2 = 32$ ms (Fig. 5*C*).

TABLE I
Comparison of I_{\min} functional properties in A431 and HEK293 cells

Property	HEK293	A431
Conductance		
Divalent cations	1.2 pS (Fig. 3C)	1.5 pS (18)
DVF	10 pS (Fig. 6B)	8.5–10 pS (19)
Mean open time	9 ms (Fig. 3D)	7.7 ms (16)
IVC		
Divalent	Linear (Fig. 3C)	Linear (19)
DVF	Linear (Fig. 6B)	Linear (19)
$P_{Ba/K}$	20 (Fig. 3C)	15 (19)
Block by Mg ²⁺	No (Fig. 3)	No (19)
Activation by		
Store-depletion	No	Yes (18,19)
InsP ₃	Yes (Fig. 3B)	Yes (18,19)
PLC	Yes (Fig. 3A)	Yes (18,19)
PIP ₂	Inhibits (Fig. 4)	Inhibits (17)
Encoded by	Member of TRP family (?)	

TABLE II
Observation frequency of different channel types in patches from HEK293 cells

Configuration	Activator	I_{\min}	I_{\max}	I_{NS}	n
c/a	UTP	56	47	10	118
c/a	TPEN	0	18	12	84
i/o	InsP ₃	18	15	0	80

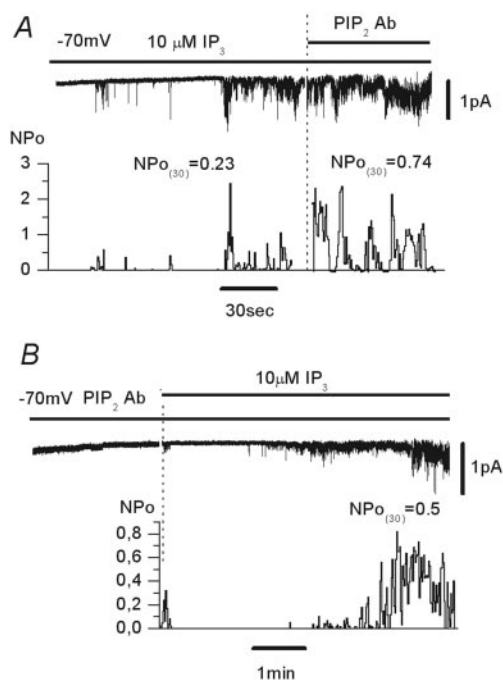


FIG. 4. PIP₂Ab enhances activity of I_{\min} channels in HEK293 cells. *A*, current trace in inside-out (*i/o*) patch recorded after application of 10 μ M InsP₃ and PIP₂Ab at -70 mV holding potential as indicated. I_{\min} NPo plot for the same experiment is shown at the bottom. NPo was averaged over 0.5-s intervals and plotted versus time in the experiment. Mean NPo was 0.23 after InsP₃ application and 0.74 after PIP₂Ab addition. Data are representative of 36 experiments. *B*, the same experiment as in *panel A* with the order of InsP₃ and PIP₂Ab additions reversed. Data are representative of 48 experiments.

What is a mechanism of I_{\max} channels activation? Similar to I_{\min} channels, I_{\max} channels could be activated by application of InsP₃ to cytosolic surface of inside-out patches from HEK293 cells in 15 out of 80 experiments (Fig. 5D) (Table II). PIP₂-sensitivity of I_{\max} channels has not been investigated in this study. These results indicated that I_{\max} channels in HEK293 cells can function as receptor-activated (ROC) channels. In our previous *i/o* patch clamp experiments with A431 cells we described InsP₃-gated channels with properties similar to

I_{\max} (13). Application of 1 mM TPEN resulted in activation of I_{\max} channels in 18 out of 84 *c/a* patches from HEK293 cells (Fig. 5E) (Table II), indicating that I_{\max} channels are store-operated. Thus, in contrast to “ROC-only” I_{\min} channels, I_{\max} channels contribute to both ROC and SOC currents in HEK293 cells.

I_{min} and I_{max} Channels Display Different Conductance for Monovalent Cations—Experiments described above suggested an existence of at least two distinct Ca²⁺ influx channel types (I_{\min} and I_{\max}) in plasma membrane of HEK293 cells. To investigate this possibility further, we performed a series of *i/o* patch clamp recordings in divalent-free media containing 140 mM Na⁺. In the absence of divalent cations, Na⁺ and other monovalent cations carry a substantial current through voltage-gated Ca²⁺ channels (35, 36). In our previous studies, we characterized monovalent currents mediated by I_{\min} channels in A431 cells (19). We found that addition of 10 μ M of InsP₃ to cytosolic surface of *i/o* patches from HEK293 cells resulted in channel activity in 12 out of 24 attempts. Two distinct channel types were recorded in these experiments (Fig. 6). In six experiments we observed 10 pS conductance channels (Fig. 6, *A* and *B*) with the properties similar to I_{\min} channels recorded in divalent-free media in A431 cells (19) (Table I). In another six experiments we observed 33 pS channels (Fig. 6, *C* and *D*). Because both I_{\min} and I_{\max} can be activated by application of InsP₃ to *i/o* patches taken from HEK293 cells (Figs. 3B and 5D), we reasoned that 10 pS channels correspond to monovalent currents via I_{\min} channels and 33 pS channels correspond to monovalent currents via I_{\max} channels.

Non-selective I_{NS} Channels Contribute to SOC Pathway in HEK293 Cells—Divalent ion selectivity of I_{\max} channels (Fig. 5B) is consistent with reversal potential of SOC currents observed in some HEK293 cells (Fig. 2D). However, other HEK293 cells displayed non-selective SOC current (Fig. 2E) with reversal potential incompatible with I_{\max} permeability properties. Are there additional store-operated channels in HEK293 cells? Careful examination of our data revealed that in 10 out of 118 attempts application of 100 μ M UTP induced activity of yet another channel type in *c/a* patches (Fig. 7A) (Table II). In contrast to I_{\min} and I_{\max} channels, the current via these channels had an outward direction when recorded at membrane potentials more positive than -10 mV. The unitary current-voltage relationship of these channels is shown on Fig. 7B. The current-voltage relationship of these channels was linear between -90 and -50 mV with the slope conductance of 5 pS. The current reversal potential was -10 mV, consistent with non-selective channels ($P_{Ba/K} = 0.4$, Equation 1). Thus, we called these channels I_{NS} (non-selective channels). Fig. 7C illustrates that the open time distribution of the UTP-evoked I_{NS} channel could be fit by a single exponential function with the time constant of 3.5 ms. Application of 2.5 μ M InsP₃ failed to induce activity of I_{NS} channels in *i/o* patches from HEK293 cells ($n = 80$) (Table II). However, in 12 out of 84 attempts application of 10 mM TPEN induced activity of I_{NS} channels in *c/a* patches (Fig. 7D and Table II). The I_{NS} channels can also be activated by loading HEK293 cells with 100 μ M BAPTA-AM (Fig. 7E) in 8 out of 20 experiments. Thus, we concluded that I_{NS} channels are store-operated and contribute to SOC currents, but not to ROC currents, in HEK293 cells. Based on similarity in ionic selectivity, it is likely that non-selective SOC current observed in some of our whole cell experiments with TPEN (Fig. 2E) is primarily carried by I_{NS} channels.

DISCUSSION

Ca²⁺ Influx Channels in HEK293 and A431 Cells—By using a combination of whole cell and single channel patch clamp recordings we identified four distinct types of endogenous

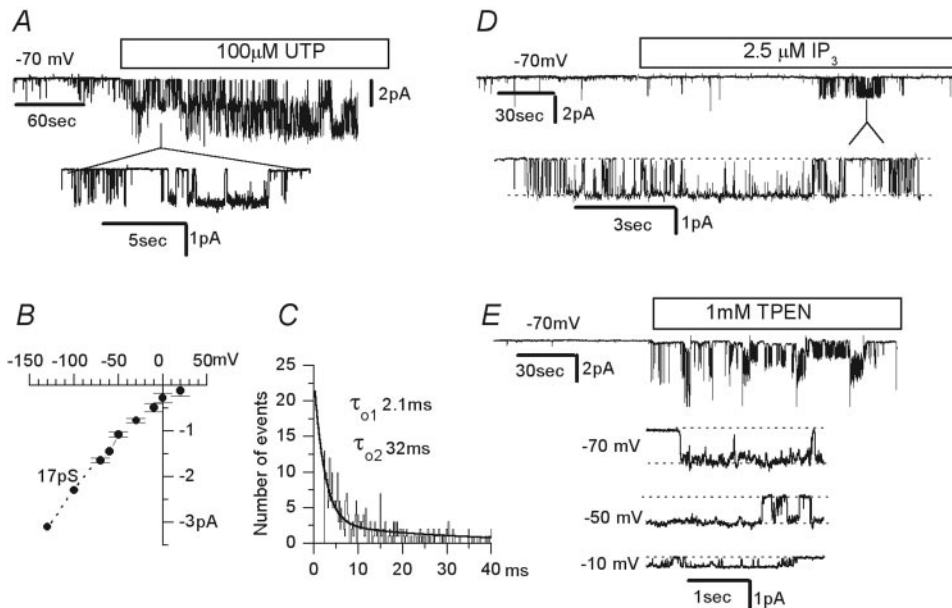


FIG. 5. I_{\max} channels in HEK293 cells. *A*, bath application of $100 \mu\text{M}$ UTP to cell-attached patches held at -70-mV membrane potential activated I_{\max} channels in the patch. The fragment of the current record is shown at the *bottom* on the expanded time scale. *B*, the mean current-voltage relationship of I_{\max} channels. Each point represents the average of UTP-, and InsP_3 -induced currents in three to eight experiments. The fit to the data points (*line*) yielded single channel conductance $\gamma = 17 \text{ pS}$ and extrapolated reversal potential $E_{\text{rev}} = +30 \text{ mV}$. *C*, an open-time histogram of I_{\max} channel. One channel was active in a given patch. Events with time duration of less than 3 ms were discarded to exclude artifactual openings from the analysis. The total number of events was 1012. The *line* represents a sum of two exponential fit to the data with time constants $\tau_{o1} = 2.1 \text{ ms}$ and $\tau_{o2} = 32 \text{ ms}$. Channel activity was recorded at membrane potential of -70 mV . Data filtered at 500 Hz . *D*, application of $2.5 \mu\text{M}$ InsP_3 to the cytosolic surface of inside-out (*i/o*) patch held at -70-mV membrane potential activated I_{\max} channels in the patch. The fragment of the current record is shown at the *bottom* on the expanded time scale. *E*, bath application of 1 mM TPEN to cell-attached (*c/a*) patches held at -70-mV membrane potential activated I_{\max} channels in the patch. The fragments of I_{\max} current records are shown at the *bottom* on the expanded time scale at membrane potentials as indicated.

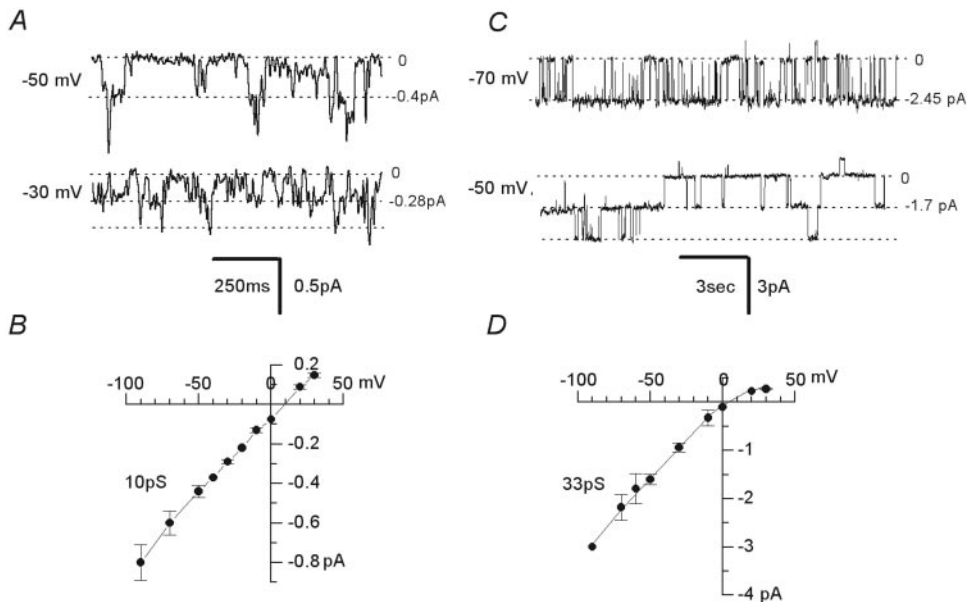


FIG. 6. Monovalent currents via I_{\min} and I_{\max} channels in HEK293 cells. Current recordings were performed in inside-out (*i/o*) patches with 140 mM Na^+ in the pipette. The channel activity was induced by addition of $10 \mu\text{M}$ InsP_3 to the bath. *A*, monovalent currents via I_{\min} channels at membrane potentials as indicated. *B*, the mean current-voltage relationship of I_{\min} channels with 140 mM Na^+ as a current carrier. At each voltage the data are shown as mean \pm S.E. ($n = 6$). The linear fit to the data points (*line*) yields single channel conductance $\gamma = 10 \text{ pS}$ and reversal potential $E_{\text{rev}} = +10 \text{ mV}$. *C*, monovalent currents via I_{\max} channels at membrane potentials as indicated. *D*, the mean current-voltage relationship of I_{\max} channels with 140 mM Na^+ as a current carrier. At each voltage the data are shown as mean \pm S.E. ($n = 5$). The fit to the data points (*line*) yields single channel conductance $\gamma = 33 \text{ pS}$ and reversal potential $E_{\text{rev}} = +5 \text{ mV}$.

Ca²⁺ influx channels in HEK293 cells: I_{CRAC} , I_{\min} , I_{\max} , and I_{NS} . Each of the channels has unique permeability properties and activation profiles. I_{CRAC} channels are highly selective for divalent cations ($P_{\text{D/M}} > 1000$) and display strong inward rectification. In HEK293 cells I_{CRAC} channels can be activated by application of PLC-linked receptor agonist such as

UTP (Fig. 2A) or by depletion of intracellular Ca²⁺ stores (Fig. 2C). In the previous studies we observed I_{CRAC} currents with similar properties in A431 cells (19). As determined in previous studies by us (19) and others (6, 37) unitary conductance of I_{CRAC} channels is too small (estimated at 24 pS) to allow single channel analysis. Thus, we have not been able to

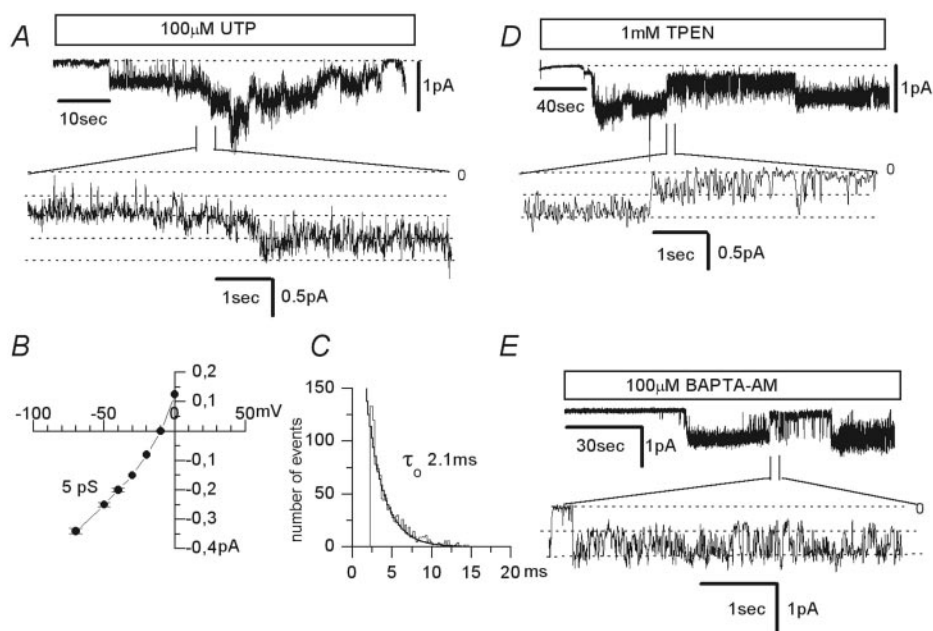


FIG. 7. I_{NS} channels in HEK293 cells. *A*, bath application of 100 μ M UTP to cell-attached (*c/a*) patches held at -70 -mV membrane potential induced I_{NS} channel activity. The fragments of current records on compressed (*top*) and on expanded (*bottom*) time scale are shown as indicated. *B*, the mean current-voltage relationship of I_{NS} channels. Each point represents the average of UTP-, TPEN-, and BAPTA-AM-induced currents in 5–10 experiments. The fit to the data points (*line*) yielded single channel conductance $\gamma = 5$ pS and reversal potential $E_{rev} = -10$ mV. *C*, an open-time histogram of I_{NS} channels. One channel was active in the patch. Events with time duration of <2 ms were discarded to exclude artifactual openings from the analysis. The total number of events was 1440. The *line* represents a single exponential fit to the data with a time constant of 2.1 ms. Channel activity was recorded at membrane potential of -70 mV. Data were filtered at 500 Hz. *D* and *E*, bath application of 1 mM TPEN (*D*) or 100 μ M BAPTA-AM (*E*) to cell-attached (*c/a*) patches held at -70 -mV membrane potential activated I_{NS} channel activity. The fragments of current records on compressed (*top*) and on expanded (*bottom*) time scale are shown as indicated.

investigate the properties of I_{CRAC} channels in HEK293 cells at the single channel level.

I_{min} channels display 1.2 pS conductance for divalent cations (Fig. 3C), 10 pS conductance for monovalent cations (Fig. 6B) and moderate selectivity for divalent cations ($P_{Ba/K} = 20$) (Fig. 3C). The conductance, permeability, and gating properties of I_{min} channels in HEK293 cells are identical to the properties of I_{min} channels that we described in A431 cells (Table I). In HEK293 cells I_{min} channels are activated by UTP (*c/a*) (Fig. 3A) or $InsP_3$ (*i/o*) (Fig. 3B), but not by store depletion (Table II). Thus, in HEK293 cells I_{min} channels function as ROC channels, but not as SOC channels. Importantly, we confirmed an existence of ROC Ca²⁺ influx pathway in HEK293 cells in Ca²⁺ imaging experiments with Ad- $InsP_3R$ -N adenovirus (Fig. 1C). Similar to A431 cells (17), I_{min} channels are functionally coupled to PIP₂ in HEK293 cells (Fig. 4). Quantitative comparison of results obtained in experiments with PIP₂Ab in inside-out patches taken from HEK293 cells (Fig. 4) and A431 cells (17, 18) shows that I_{min} channels are under stronger tonic inhibition by PIP₂ in HEK293 cells than in A431 cells. Most likely the explanation of this phenomenon is higher levels of global or local PIP₂ levels in HEK293 cells.

I_{max} channels display 17-pS conductance for divalent cations (Fig. 5B), 33-pS conductance for monovalent cations (Fig. 6D), and less selective for divalent cations than I_{min} channels ($P_{Ba/K} = 4$) (Fig. 5B). In HEK293 cells I_{max} channels can be activated by UTP (*c/a*) (Fig. 5A), $InsP_3$ (*i/o*) (Fig. 5D), or by store depletion (Fig. 5E) (Table II). Thus, in HEK293 cells I_{max} channels function as both ROC and SOC channels. In addition to I_{min} and I_{max} , we also identified non-selective I_{NS} channels with 5-pS conductance (Fig. 7B) and $P_{Ba/K} = 0.4$ (Fig. 7B). I_{NS} channels are not $InsP_3$ -gated but can be activated by depletion of Ca²⁺ stores (Fig. 7, *D* and *E*) (Table II). Thus, in HEK293 cells I_{NS} channels function as SOC channels but not as ROC channels. In A431 cells we also observed I_{max} and I_{NS} channels

(Ref. 13 and data not shown), but in our recent studies we focused primarily on I_{min} (14, 15, 18, 19).

Obtained results lead us to conclude that in HEK293 cells ROC currents are supported by a combination of I_{min} and I_{max} channels (with the possible contribution of I_{CRAC}), and SOC currents are supported by I_{CRAC} , I_{max} , and I_{NS} channels. Single channel recordings reveal that each of these channels displays unique conductance and selectivity properties. Although used widely, Ca²⁺ imaging (Fig. 1) and whole cell currents (Fig. 2) report combined Ca²⁺ influx via multiple channel types. Thus, conclusions regarding ion selectivity and activation mechanisms of ROC and SOC currents based on Ca²⁺ imaging and whole cell experiments can be misleading without knowledge of single channel properties of channels supporting these currents.

The molecular identity of channels encoding I_{CRAC} Ca²⁺ influx channels in HEK293 and A431 cells remains unknown, but the members of TRP family are the most likely candidates for the role of I_{min} , I_{max} , and I_{NS} channels. HEK293 cells express endogenous TRPC1, TRPC3, TRPC4, and TRPC6 proteins (28–30). Our preliminary molecular analysis (in collaboration with William Schilling) confirmed an expression of multiple TRPC isoforms in A431 cells. The conductance and selectivity properties of I_{max} and I_{NS} channels are consistent with functional properties displayed by TRPC proteins when expressed as homo- or heteromers (3, 7, 9–12). In particular, conductance and selectivity of I_{max} channels resembles properties of the channels formed by TRPC1 when expressed in the human submandibular gland cell line (38). Previous Ca²⁺ imaging studies demonstrated that suppression of TRPC4 expression in HEK293 cells by RNA interference lead to reduction of ROC, but not SOC Ca²⁺ influx pathway (30). In contrast, suppression of TRPC3 expression in the same study affected both ROC and SOC Ca²⁺ influx pathways in HEK293 cells (30). Thus, TRPC3 and TRPC4 subunits are likely candidates to encode I_{max} and I_{NS} channels in HEK293 cells. Single channel

conductance of I_{min} channels is lower and selectivity for divalent cations is higher than the range of values reported for the channels formed by TRPC subunits. Thus, I_{min} channels may be encoded by a more selective member of TRP family such as TRPV6 (39–42). Application of molecular techniques, such as RNA interference (43), should help to clarify molecular composition of I_{min}, I_{max}, and I_{NS} Ca²⁺ influx channels in HEK293 and A431 cells (30, 44). In addition, recently discovered specific SOC inhibitors tetrapandin peptides (45) will be useful in identification of SOC-supporting channels in HEK293 and A431 cells.

From functional analysis we concluded that I_{min} channels display identical functional properties in A431 and HEK293 cells (Table I) and most likely encoded by the same member of TRP family in both types of cells. However, I_{min} channels are store-operated in A431 cells (18, 19) and store-independent in HEK293 cells (Table II). Conflicting results regarding store dependence of TRP-supported channels have been obtained by a variety of groups (3, 7, 9–12). Usually these discrepancies are interpreted as an artifact of overexpression system. In our studies we find that endogenous I_{min} channels are store-dependent in A431 cells and store-independent in HEK293 cells. Thus, most likely coupling of I_{min} channels to store depletion depends on an accessory protein that is present in A431 cells but is absent in HEK293 cells. In addition, different InsP₃R isoforms expressed in A431 and HEK293 cells may affect store dependence of I_{min} activation. Definitive molecular identification of I_{min}-encoding proteins is required to address this issue.

Acknowledgments—We thank Thomas Südhof for InsP₃R1 plasmid, Bert Vogelstein for generously providing AdEasy system components, and Konstantin Gusev for technical assistance.

REFERENCES

- Parekh, A. B., and Penner, R. (1997) *Physiol. Rev.* **77**, 901–930
- Putney, J. W., Jr., Broad, L. M., Braun, F. J., Lievreumont, J. P., and Bird, G. S. (2001) *J. Cell Sci.* **114**, 2223–2229
- Venkatachalam, K., van Rossum, D. B., Patterson, R. L., Ma, H. T., and Gill, D. L. (2002) *Nat. Cell Biol.* **4**, E263–272
- Hoth, M., and Penner, R. (1992) *Nature* **355**, 353–356
- Premack, B. A., McDonald, T. V., and Gardner, P. (1994) *J. Immunology* **152**, 5226–5240
- Zweifach, A., and Lewis, R. S. (1993) *Proc. Natl. Acad. Sci. U. S. A.* **90**, 6295–6299
- Nilius, B., and Droogmans, G. (2001) *Physiol. Rev.* **81**, 1415–1459
- Clapham, D. E. (1996) *Neuron* **16**, 1069–1072
- Montell, C., Birnbaumer, L., and Flockerzi, V. (2002) *Cell* **108**, 595–598
- Birnbaumer, L., Zhu, X., Jiang, M., Boulay, G., Peyton, M., Vannier, B., Brown, D., Platano, D., Sadeghi, H., Stefani, E., and Birnbaumer, M. (1996) *Proc. Natl. Acad. Sci. U. S. A.* **93**, 15195–15202
- Zitt, C., Halaszovich, C. R., and Luckhoff, A. (2002) *Prog. Neurobiol.* **66**, 243–264
- Clapham, D. E., Runnels, L. W., and Strubing, C. (2001) *Nat. Rev. Neurosci.* **2**, 387–396
- Mozhayeva, G. N., Naumov, A. P., and Kuryshev, Y. A. (1990) *FEBS Lett.* **277**, 233–234
- Kiselyov, K. I., Mamin, A. G., Semyonova, S. B., and Mozhayeva, G. N. (1997) *FEBS Lett.* **407**, 309–312
- Kiselyov, K. I., Semyonova, S. B., Mamin, A. G., and Mozhayeva, G. N. (1999) *Pflugers Arch.* **437**, 305–314
- Zubov, A. I., Kaznacheeva, E. V., Nikolaev, A. V., Alexeenko, V. A., Kiselyov, K., Muallem, S., and Mozhayeva, G. N. (1999) *J. Biol. Chem.* **274**, 25983–25985
- Kaznacheeva, E., Zubov, A. N., Nikolaev, A., Alexeenko, V., Bezprozvanny, I., and Mozhayeva, G. N. (2000) *J. Biol. Chem.* **275**, 4561–4564
- Kaznacheeva, E., Zubov, A., Gusev, K., Bezprozvanny, I., and Mozhayeva, G. N. (2001) *Proc. Natl. Acad. Sci. U. S. A.* **98**, 148–153
- Gusev, K., Glouchankova, L., Zubov, A., Kaznacheeva, E., Wang, Z., Bezprozvanny, I., and Mozhayeva, G. N. (2003) *J. Gen. Physiol.* **122**, 81–94
- Strubing, C., Krapivinsky, G., Krapivinsky, L., and Clapham, D. E. (2001) *Neuron* **29**, 645–655
- Hurst, R. S., Zhu, X., Boulay, G., Birnbaumer, L., and Stefani, E. (1998) *FEBS Lett.* **422**, 333–338
- Kiselyov, K., Xu, X., Mozhayeva, G., Kuo, T., Pessah, I., Mignery, G., Zhu, X., Birnbaumer, L., and Muallem, S. (1998) *Nature* **396**, 478–482
- Venkatachalam, K., Zheng, F., and Gill, D. L. (2003) *J. Biol. Chem.* **278**, 29031–29040
- Schaefer, M., Plant, T. D., Stresow, N., Albrecht, N., and Schultz, G. (2002) *J. Biol. Chem.* **277**, 3752–3759
- Yamada, H., Wakamori, M., Hara, Y., Takahashi, Y., Konishi, K., Imoto, K., and Mori, Y. (2000) *Neurosci. Lett.* **285**, 111–114
- Inoue, R., Okada, T., Onoue, H., Hara, Y., Shimizu, S., Naitoh, S., Ito, Y., and Mori, Y. (2001) *Circ. Res.* **88**, 325–332
- Shi, J., Mori, E., Mori, Y., Mori, M., Li, J., Ito, Y., and Inoue, R. (2004) *J. Physiol.* **561**, 415–432
- Garcia, R. L., and Schilling, W. P. (1997) *Biochem. Biophys. Res. Commun.* **239**, 279–283
- Groschner, K., Hingel, S., Lintschinger, B., Balzer, M., Romanin, C., Zhu, X., and Schreiber, W. (1998) *FEBS Lett.* **437**, 101–106
- Wu, X., Babnigg, G., Zagranichnaya, T., and Villereal, M. L. (2002) *J. Biol. Chem.* **277**, 13597–13608
- He, T. C., Zhou, S., da Costa, L. T., Yu, J., Kinzler, K. W., and Vogelstein, B. (1998) *Proc. Natl. Acad. Sci. U. S. A.* **95**, 2509–2514
- Mignery, G. A., Newton, C. L., Archer, B. T., and Sudhof, T. C. (1990) *J. Biol. Chem.* **265**, 12679–12685
- Hille, B. (2001) *Ionic Channels of Excitable Membranes*, 3rd Ed., p. 448, Sinauer Associates, Sunderland, MA
- Uchiyama, T., Yoshikawa, F., Hishida, A., Furuichi, T., and Mikoshiba, K. (2002) *J. Biol. Chem.* **277**, 8106–8113
- Hess, P., and Tsien, R. W. (1984) *Nature* **309**, 453–456
- Almers, W., McCleskey, E. W., and Palade, P. T. (1984) *J. Physiology* **353**, 565–583
- Prakriya, M., and Lewis, R. S. (2002) *J. Gen. Physiol.* **119**, 487–507
- Liu, X., Wang, W., Singh, B. B., Lockwich, T., Jadlowiec, J., O'Connell, B., Wellner, R., Zhu, M. X., and Ambudkar, I. S. (2000) *J. Biol. Chem.* **275**, 3403–3411
- Vennekens, R., Hoenderop, J. G., Prenen, J., Stuijver, M., Willems, P. H., Droogmans, G., Nilius, B., and Bindels, R. J. (2000) *J. Biol. Chem.* **275**, 3963–3969
- Nilius, B., Vennekens, R., Prenen, J., Hoenderop, J. G., Bindels, R. J., and Droogmans, G. (2000) *J. Physiol.* **527**, 239–248
- Suzuki, M., Ishibashi, K., Ooki, G., Tsuruoka, S., and Imai, M. (2000) *Biochem. Biophys. Res. Commun.* **274**, 344–349
- Yue, L., Peng, J. B., Hediger, M. A., and Clapham, D. E. (2001) *Nature* **410**, 705–709
- Elbashir, S. M., Harborth, J., Lendeckel, W., Yalcin, A., Weber, K., and Tuschl, T. (2001) *Nature* **411**, 494–498
- Ma, R., Rundle, D., Jacks, J., Koch, M., Downs, T., and Tsiokas, L. (2003) *J. Biol. Chem.* **278**, 52763–52772
- Shalabi, A., Zamudio, F., Wu, X., Scalconi, A., Possani, L. D., and Villereal, M. L. (2004) *J. Biol. Chem.* **279**, 1040–1049